

The Infrared Einstein Ring in the Gravitational Lens
MG 1131+0456
and the Death of the Dusty Lens Hypothesis¹

C. S. Kochanek^(a),

E. E. Falco^(a), C. D. Impey^(b), J. Lehar^(a), B. A. McLeod^(a)

H.-W. Rix^(b), C. R. Keeton^(b) and C.Y. Peng^(b)

^(a) Harvard-Smithsonian Center for Astrophysics, 60 Garden St., Cambridge, MA 02138
email: ckochanek, efalco, jlehar, bmcleod@cfa.harvard.edu

^(b) Steward Observatory, University of Arizona, Tucson, AZ 85721
email: cimpey, rix, ckeeton, cyp@as.arizona.edu

Received _____; accepted _____

Submitted to Astrophysical Journal

¹Based on Observations made with the NASA/ESA Hubble Space Telescope, obtained at the Space Telescope Science Institute, which is operated by AURA, Inc., under NASA contract NAS 5-26555.

ABSTRACT

We have obtained and modeled new NICMOS images of the lens system MG 1131+0456, which show that its lens galaxy is an H= 18.6 mag, transparent, early-type galaxy at a redshift of $z_l \simeq 0.85$; it has a major axis effective radius $R_e = 0''.68 \pm 0''.05$, projected axis ratio $b/a = 0.77 \pm 0.02$, and major axis PA= $60^\circ \pm 2^\circ$. The lens is the brightest member of a group of seven galaxies with similar R–I and I–H colors, and the two closest group members produce sufficient tidal perturbations to explain the ring morphology. The host galaxy of the MG 1131+0456 source is a $z_s \gtrsim 2$ ERO (“extremely red object”) which is lensed into optical and infrared rings of dramatically different morphologies. These differences imply a strongly wavelength-dependent source morphology that could be explained by embedding the host in a larger, dusty disk. At $1.6\mu\text{m}$ (H), the ring is spectacularly luminous, with a total observed flux of H= 17.4 mag and a de-magnified flux of 19.3 mag, corresponding to a $1\text{--}2L_*$ galaxy at the probable source redshift of $z_s \gtrsim 2$. Thus, it is primarily the stellar emission of the radio source host galaxy that produces the overall colors of two of the reddest radio lenses, MG 1131+0456 and B 1938+666, aided by the suppression of optical AGN emission by dust in the source galaxy. The dusty lens hypothesis — that many massive early-type galaxies with $0.2 \lesssim z_l \lesssim 1.0$ have large, uniform dust opacities — is ruled out.

Subject headings: gravitational lensing: cosmology – galaxies: evolution – galaxies: photometry – individual objects: MG 1131+0456 – extinction

1. INTRODUCTION

The lens galaxies of the ~ 30 gravitational lenses with $\Delta\theta \gtrsim 1''0$ constitute a sample of massive galaxies selected from diverse but generally low density environments in the redshift range $0.2 \lesssim z_l \lesssim 1.0$. As such, they complement the evolutionary studies of galaxies in rich clusters across the same redshift range. Stanford et al. (1995, 1998) and Ellis et al. (1997) have shown that morphologically identified early-type galaxies in rich clusters have colors that match passively evolving stellar population models even at $z \simeq 1$. These galaxies obey fundamental-plane relations, and the directly measured evolution of the mass-to-light ratio (M/L) is well matched to the changes expected from passive evolution (e.g. Kelson et al. 1997, van Dokkum et al. 1998). Keeton, Kochanek & Falco (1998) showed that the gravitational lens galaxies show the same passive evolution in both color and M/L as their counterparts in rich clusters. While there are fewer lens galaxies, they have the great advantage of precisely measured individual masses at any redshift without the complications of interpreting stellar dynamics.

Studies of red galaxies with $z \gtrsim 1$ are more difficult due to the lack of identified clusters and the difficulty in obtaining spectra of red objects (as compared to blue, star-forming, emission line objects). In particular, the properties of the ERO (extremely red object) population with $R-K \gtrsim 6$ mag are poorly understood. For example, LBDS 53W091 at $z = 1.55$ (Dunlop et al. 1995, Spinrad et al. 1997) is believed to be a nearly dust free, early-type galaxy whose old stellar population sets strong limits on the epoch of star formation and the age of the universe at that epoch. On the other hand, Graham & Dey (1996) argue that the less radio luminous galaxy HR 10 at $z = 1.44$ is an intense starburst which is heavily obscured by dust. Quasars and radio sources also show a wide range of optical colors. Flat-spectrum radio sources range from very blue quasars to colors as red as those of the EROs (Webster et al. 1995), with the optically selected quasars concentrated on the blue tail of the distribution. The red colors can be due to the extinction in the host galaxy (e.g. Wills et al. 1992), extinction in intervening galaxies or protogalaxies (e.g. Heisler & Ostriker 1988, Fall & Pei 1993), the continuation of steep synchrotron emission from the compact radio source (e.g. Impey & Neugebauer 1988), or the stellar light of the host galaxy. The last possibility was assumed by Dunlop et al. (1996) when they selected LBDS 53W091.

Gravitational lens systems also offer a unique opportunity to probe the dust content of distant galaxies, because the lensed images can be used to estimate the extinction differences on paths separated by 1–10 kpc at typical redshifts (e.g. Nadeau et al. 1991). Further, differences between the statistics of radio and optically selected lens samples can be used to estimate the mean extinction of the population (Falco, Kochanek & Muñoz 1998). In this approach there is no need to untangle the amount and distribution of dust from stellar population effects. Surveys of radio-selected lenses by Annis & Luppino (1993) and Malhotra, Rhoads & Turner (1997) showed that a significant number had very red optical to infrared colors, particularly the radio-selected lenses MG 0414+0534 (Hewitt

et al. 1992, Lawrence et al. 1995, Annis & Luppino 1993), MG 1131+0456 (Hewitt et al. 1988, Annis 1992, Larkin et al. 1994), and B 1938+666 (King et al. 1997, Rhoads, Malhotra, & Kundic 1996). With typical R–K colors of 6–7 mag, these three lenses lie near the extreme red edge of the color distribution found by Webster et al. (1995) and have colors typical of the EROs. Of the three, only MG 0414+0534 provides direct evidence for dust: the optical images are dominated by four point-like images (Hewitt et al. 1992) of a highly reddened ($A_V \sim 7$), $z_s = 2.64$ quasar identified by its broad $H\alpha$ line in the infrared (Lawrence et al. 1995). In the other two cases the dust is inferred from the red colors by assuming that the source should have an intrinsically blue quasar spectrum due to the presence of the radio source, but there is no direct support from a well-resolved image or an analyzable spectrum. The two surveys of lens colors reached quite different conclusions. Malhotra et al. (1997) advocated dusty lenses as the origin of the red colors, while Annis & Luppino (1993) advocated reddening in the source combined with stellar emission from the host galaxy.

With the advent of WFPC2 and NICMOS it became possible to image directly the lenses and study the morphology and colors of the host galaxies. Emission by the host galaxy is seen in the optical for MG 1131+0456 (Hammer et al. 1991, Keeton et al. 1998), MG 0414+0534 (Falco et al. 1997), BRI 0952–0115 (Lehár et al. 1998), B 1600+434 (Keeton et al. 1998), B 1608+656 (Fassnacht et al. 1996) and FSC 10214+4724 (Eisenhardt et al. 1996) and in the infrared for B 1938+666 (King et al. 1998) PG 1115+080 (Impey et al. 1998), HE 1104–1805 (Lehár et al. 1998) and H 1413+117 (McLeod et al. 1998b). Near-infrared data have the natural advantage for studying host galaxies, because the H filter measures flux emitted longward of the 4000\AA break for all source redshifts $z_s \lesssim 3$. In contrast, the I-band records only the relatively faint rest-UV flux for redshifts $z_s \gtrsim 1$.

MG 1131+0456 was the first Einstein ring lens to be discovered (Hewitt et al. 1988). It consists of two images of a radio core and an Einstein ring created by the radio jet crossing the astroid caustic of the lens. The ring is very elliptical with a major axis diameter of $2''.05$ between the radio cores. Chen & Hewitt (1993) and Hewitt, Chen & Messier (1995) produced greatly improved radio images and found that the cores are weakly variable. The optical counterpart to the system is faint ($m_R \simeq 22$ mag) and red. Hammer et al. (1991) suggested the lens was an early-type galaxy at $z_l \simeq 0.85$ and that there was an optical Einstein ring surrounding the central lens galaxy. Infrared imaging by Annis (1992) and Larkin et al. (1994) showed that the counterparts of the radio cores are very red and that there is a concentration of galaxies projected within $20''$ of the lens. Larkin et al. (1994) attributed the red source color to extinction in the lens galaxy, while Annis & Luppino (1993) interpreted it as source galaxy flux. Kochanek et al. (1989) and Chen, Kochanek & Hewitt (1995) modeled the radio emission to reconstruct the lens mass distribution. Chen et al. (1995) found that the shear axis of the best fit models matched the orientation of the tidal shear produced by the two nearby galaxies found by Annis (1992), and Keeton et al. (1998) found that the shear axis of the models was misaligned with respect to the major

axis of the lens galaxy.

In this paper we present new H band images of MG 1131+0456, obtained with NICMOS as part of the Center for Astrophysics/Arizona Space Telescope Lens Survey (CASTLES). These images permit a detailed study of the lensing galaxy, the source galaxy, the dust content of both lens and source, and allow us to estimate the redshifts of a galaxy group projected nearby. We start by describing the data (§2.1) and the spectrophotometric models we use for interpretation (§2.2). Next, we describe qualitatively the wavelength dependent structure of the source (§2.3) and follow that with a detailed discussion of the lens galaxy (§2.4) and the surrounding group (§2.5). Next we derive a new lens model for the system (§3.1) and then use the model to reconstruct the intrinsic source structure (§3.2). In §4 we discuss the extinction in MG 1131+0456 and its consequences for hypotheses about the role of dust in lens systems. Finally, we summarize our findings in §5.

2. Observations and Data Analysis

2.1. HST Photometry

Using the NIC2 camera on HST we observed MG 1131+0456 through the F160W filter, which corresponds roughly to the H band. For two orbits, we obtained four dithered exposures each, for a total exposure time of 5120 sec. The NICMOS data were reduced using the “nicred” package of custom C-program and IRAF² scripts developed for this project (McLeod 1997, Lehár et al. 1998). We also re-analyzed two orbits of HST WFPC2 observations of MG 1131+0456 which had been acquired earlier (Keeton et al. 1998). The target was observed for 8100 sec through the F675W filter (R-band), and 10500 s through the F814W filter (I-band). In each case, the orbit had been split into several sub-exposures to remove cosmic ray events. Details of our WFPC2 reduction are also given elsewhere (Lehár et al. 1998). The 8 GHz radio image is from Chen & Hewitt (1993).

Figures 1 and 2 show the PC field (R and I-band co-added) and NIC2 field around the lens galaxy. We used SExtractor (Bertin & Arnouts 1997) to catalog the objects in the fields, using the default settings for most software options. The total object magnitudes were estimated using Kron-type automatic apertures, and their colors were determined using fixed circular apertures (of diameter 0''.3, 0''.56, 1''.0, or 1''.7, chosen to exceed twice the rms object size along its major axis in the I-band exposure). In computing the object magnitudes, we used zero-points of 22.08 for R, 21.69 for I (Holtzman et al. 1995, gain of 7, corrected to infinite aperture) and 21.80 for H, which correspond to 1 count/sec. We only

² IRAF (Image Reduction and Analysis Facility) is distributed by the National Optical Astronomy Observatories, which are operated by the Association of Universities for Research in Astronomy, Inc., under contract with the National Science Foundation.

cataloged objects in the PC field which were detected in both WFPC2 bands. These objects are shown in Figures 3 and 4 and listed in Table 1, where we have labeled them in order of decreasing I-band flux. In our nomenclature the main lens galaxy is G and the remaining galaxies in the PC field are labeled G1, G2 \dots in order of increasing I magnitude. Thus the two nearby perturbing galaxies found by Annis (1992) are C=G15 and D=G9.

2.2. Photometric Models of Galaxy Evolution

To interpret the colors and magnitudes of the galaxies detected in the field, we used spectrophotometric models (Bruzual & Charlot 1993) to compute K and evolutionary corrections for present-day L_* galaxies (*i.e.* galaxies of different morphological types with $M_B = -19.9 + 5 \log h_{100}$ at $z = 0$). These corrections allow us to estimate the magnitudes and colors of such galaxies at any other redshifts. For all galaxy types we assumed star-formation histories (SFH) that start at $z_f = 5$, in three different cosmologies: $\Omega_0 = 1$ ($\Lambda_0 = 0$), $\Omega_0 = 0.3$ ($\Lambda_0 = 0$) and $\Omega_0 = 0.3$ ($\Lambda_0 = 0.7$). For early-type galaxies, we modeled the SFH either by an initial “burst” of constant star formation that is truncated after 1 Gyr, or by an “E/S0” model, which has an exponentially decaying star formation rate, $e^{-t/1\text{Gyr}}$. For spiral galaxies, we used a star formation rate proportional to the gas fraction, where the proportionality constant was taken from Guiderdoni & Rocca-Volmerange (1988) and decreases from Sa to Sb to Sc. We assumed a Salpeter IMF for the burst and E/S0 models, and a Scalo IMF for the spiral models (see Keeton et al. 1998 for details). To predict the broad-band fluxes, the resulting energy distributions were convolved with the F675W, F814W, and F160W filter transmission curves.

Figures 3 and 4 show the observed color-magnitude and color-color diagrams for the cataloged galaxies, along with these spectrophotometric models for $\Omega_0 = 0.3$ ($\Lambda_0 = 0.7$). To make the comparison, we de-reddened the observed photometry, accounting for galactic foreground extinction of $E(B - V) = 0.036$ (Schlegel, Finkbeiner & Davis 1998). Figure 3 also shows the R and I photometry for galaxies detected over the full area of the WF/PC images using open triangles, highlighting the objects in the NIC2 field by solid points. The curves show the predicted magnitude and color of an L_* galaxy as a function of redshift (with the line pattern changing every $\Delta z = 0.5$). For brighter (fainter) galaxies the corresponding curves shift horizontally to the left (right).

2.3. Wavelength Dependent Morphology of the System Lens

The wavelength dependent morphology of the MG 1131+0456 lens system is illustrated in Figure 5, which shows the 8 GHz map (Chen & Hewitt 1993) along with H, I, and R images, centered on the lens galaxy. Note that the R and I images are slightly smoothed to enhance the visibility of faint features and that the images were registered using the center of

the lens galaxy ($= D_R$ at 8 GHz). The flux fraction arising from the lens galaxy, the source galaxy, and the active source nucleus all change dramatically as a function of wavelength, even among the optical and near-IR images. We need to describe the morphology in detail, because of the complexity of structures and because the nomenclatures for the ring features differ between the optical and the radio. The radio cores seen at low frequency (8 GHz and below) are A_R and B_R where the subscript R denotes a radio feature. At higher frequencies (15 GHz and above), the A_R core splits into two components A_{R1} and A_{R2} , where A_{R1} and B_R correspond to the active nucleus (Chen & Hewitt 1993, Chen et al. 1995). In addition to the cores and the ring, there is an apparently unlensed radio lobe C_R to the Southwest, and a central image D_R . We see the lens galaxy G in both the optical and infrared images, as well as the two perturbing galaxies C=G15 and D=G9. At the locations of the radio cores we see two peaks in the infrared, but nothing in the optical. The infrared peaks A and B correspond to the locations of the radio cores A_{R1} and B when we register the central radio component D_R on the center of the lens galaxy. We label the extended peaks seen in the infrared S_A and S_B , and identify them with two images of the central regions of the host galaxy. The overall structure of the ring differs in every image. The radio source is imaged into a complete, thin ring because the extended radio source covers little area (Kochanek et al. 1989, Chen et al. 1995). The thickness of the infrared ring means that the extended infrared source is much larger than the radio source, and the peak of the extended emission is clearly offset from the active nucleus. The optical source must be smaller and offset from both the active nucleus and the center of the extended infrared source to produce the observed partial rings.

2.4. Structure of the Dominant Lens Galaxy

As the R, I and H images reveal, the lens is an early-type galaxy, which is well fit by a de Vaucouleurs profile with major axis effective radius $R_e = 0''.68 \pm 0''.05$, axis ratio $b/a = 0.77 \pm 0.02$, and major axis position angle $60^\circ \pm 2^\circ$ in all three filters. Attempts to fit the profile with an exponential disk led to significantly higher residuals. The lens galaxy colors of I–H = 2.68 mag and R–I = 1.28 mag (see Figures 3 and 4) are well matched to the predictions of the initial burst or the E/S0 photometric models at a redshift of $0.8 \lesssim z_l \lesssim 1.0$, quite close to the redshift previously estimated by Hammer et al. (1991) of $z_l = 0.85$. If we map the galaxy back onto the fundamental plane as observed in nearby clusters, we estimate that the lens redshift is $z_l = 0.89 \pm 0.03$ at $1-\sigma$ (± 0.07 at $2-\sigma$). We will adopt the Hammer et al. (1991) redshift and the initial burst photometric model for the remainder of the discussion. The initial burst models predict $m_H = 18.0$ (18.4) for an L_* galaxy and $\Omega_0 = 1$ (0.3 flat), close to the observed $m_H = 18.57$ for the lens. The effective radius is $6.4h_{65}^{-1}$ ($8.2h_{65}^{-1}$) kpc for $\Omega_0 = 1$ (0.3 flat), compared to $R_{e*} = (6.2 \pm 1.5)h_{65}^{-1}$ kpc scale length for an L_* early-type galaxy in local samples (*e.g.* Jorgensen et al. 1992) for $H_0 = 65h_{65} \text{ km s}^{-1} \text{ Mpc}^{-1}$.

The red color of the lens best matches both the E/S0 and initial burst spectrophotometric models. Dust in the lens galaxy probably cannot explain its colors. For a rest frame $R_V = 3.1$ extinction curve, the lab-frame extinction coefficients for our filters are $R_{F675W} = 4.82$, $R_{F814W} = 4.11$, and $R_{F160W} = 1.59$ using the Cardelli et al. (1989) extinction curve model. If we uniformly mix dust into the galaxy using the simple model that the overall flux is attenuated by $(1 - e^{-\tau})/\tau$ where τ is the total optical depth of the dust through the galaxy, we can compute the intrinsic colors and magnitudes of the lens galaxy. In the color-color diagram the lens shifts to the colors of a later type galaxy at essentially the same redshift, but in the color-magnitude diagram the galaxy becomes far too luminous for any galaxy at that redshift (see Figures 3 and 4). Compared to a dust screen, dust mixed with stars has little effect on the colors compared to the luminosity, and more sophisticated models (e.g. Witt et al. 1992) for the effects of extinction tend to further reduce the color changes. Because the lens galaxy is already an L_* galaxy, the extinction required by the “dusty lens” hypothesis for the red colors of the system would make the lens galaxy anomalously luminous for any realistic extinction model. Therefore we can rule out a very dusty lens galaxy independently of the properties of the lensed source.

2.5. Lensing Galaxy Group

The galaxies G, G3, G5, G7, G8, G9=D and G15=C form an isolated cluster in both the color-magnitude and color-color diagrams for the field (see Table 1 and Figures 3 & 4). This result strongly suggests that they are early-type galaxies, with a range of 10 in H luminosity, that form a group or cluster at the lens redshift. All these galaxies have the colors of passively-evolving models and there are no candidates for late-type group members in the NIC2 field. This is consistent with the findings in rich clusters at comparable redshifts (Stanford et al. 1998). In the flanking WF/PC fields we cannot distinguish late-type group members from lower redshift and luminosity galaxies based on the I–R color alone. No similar concentration of galaxies is seen in the surrounding WF fields. Nearly 50% (6 of 13) of all galaxies in the PC field with $20.0 < m_I < 23.5$ fall in the range $1.0 < R-I < 1.5$, while in the adjacent fields that fraction is only 12%, or 12 of 104 (see Figure 3). Galaxy C=G15 is peculiar because of its relatively bluer R–I color and redder I–H color, and it may be a representative of the “faint, red outlier galaxy” population (Moustakas et al. 1997). The reddest galaxy in the field besides the lensed source is G31, with $R-H = 5.3$ ($R-K' > 4.7$ in Annis (1992)).

Chen et al. (1995) noted that the two galaxies C and D had the locations and relative fluxes needed to produce the external shear required to fit the 8 GHz radio ring. However, they could not produce the required *amplitude* of the tidal perturbation if they scaled the masses of galaxies C and D to the main lens G using the Faber-Jackson (1976) relation and the published K' magnitudes (Annis 1992). We now know, however, that the earlier IR magnitudes for G were gross overestimates because they were ignorant of the existence of

the ring (see Figure 5), and that C and D are 26% and 12% of the luminosity of G rather than 3% and 2% respectively. The Faber-Jackson (1976) relation now predicts that C and D have the masses required to produce the amplitude and orientation of the external shear in the Chen et al. (1995) lens models.

3. Models

3.1. Lensing Mass Distribution

In principle one could use the radio, near-IR and optical images of the MG 1131+0456 system simultaneously to constrain the lensing mass distribution. However, the use of the R, I and H images for this purpose is complicated, because the source and lens emission overlap in the images. Therefore, we determine the lens mass distribution only from the lensed radio image, following Chen et al. (1995). However, our new NICMOS data serve as improved constraints on the positions and relative luminosities of the three relevant lens galaxies. The mass model used to fit to the 8 GHz data consists of three singular isothermal spheres, located at the positions of galaxies G, C, and D. We then fit the radio ring using 6 Gaussian source components as an approximation to a true non-parametric source reconstruction. To keep the procedure computationally feasible we restricted ourselves to circularly symmetric potentials for each galaxy. The best fit yields critical radii of $b_G = 0''.819$, $b_C = 0''.259$, and $b_D = 0''.367$ for the three galaxies and the residuals are comparable to those of the best models found by Chen et al. (1995).

We can estimate the tidal perturbation or external shear produced by the other galaxies in the PC field at the location of the primary lens G by assuming that the galaxies are at the same redshift as G and scaling their critical radii relative to the critical radius of G (see §3.1) with luminosity L using the Faber-Jackson (1976) relation ($b \propto L^{1/2}$). Thus a galaxy of luminosity L at angular distance r from G produces an estimated tidal shear of $\gamma_T = (1/2)(b_G/r)(L/L_G)^{1/2}$ assuming a singular isothermal sphere mass distribution. The shear estimate will be overestimated if the galaxy halo is truncated on scales smaller than the distance r , or if the galaxy is a later type than the lens galaxy. Redshift differences can lead to both over and underestimates. Table 1 gives the tidal shears for the objects in the PC field using the I magnitudes to estimate the relative luminosities. The γ_T values give a simple synopsis of which galaxies may be important as perturbations, although not all galaxies with large values for γ_T will be real sources of perturbations. For example, galaxy G1 is an early-type galaxy at a significantly lower redshift whose perturbation strength is greatly exaggerated.

For the group members the shear estimates should be reasonably accurate. Equivalently we can predict the relative velocity dispersions (or critical radii) of G, C, and D from their relative luminosities, and with the newly determined magnitude of G we would expect to

find $b_C = 0''.35 \pm 0''.08$ and $b_D = 0''.26 \pm 0''.06$ for $b_G = 0''.82$. The uncertainties are based on the observed scatter of 0.5 mag in the luminosity-separation relation (Keeton et al. 1988), and we have used the H band flux ratios rather than the I band flux ratios. Thus the luminosity-predicted critical radii are in reasonable agreement with the ones derived directly from the lens model. The colors of galaxy C are peculiar (see §2.5) so it is not surprising that it shows a larger discrepancy than galaxy D. We can quantify the tidal fields of the galaxies by their external shears of $\gamma_C = 0.049$ and $\gamma_D = 0.054$ or their total combined shear of $\gamma_{CD} = 0.077$. The remaining group galaxies individually contribute $\gamma_T = 0.01$ to $\gamma_T = 0.02$ but their tensor shear contributions largely cancel, leaving a net additional shear of only $\gamma_T < 0.01$. Moreover, they are $50h_{65}^{-1}$ to $75h_{65}^{-1}$ kpc distant from the lens, so the likely tidal truncation of the galaxy halos on the scale of the member separations would further reduce their contribution.

In contrast to Chen et al. (1995) we represented the galaxies C and D by singular isothermal spheres rather than the lowest order term in a tidal expansion of the gravitational potential. The higher order terms significantly distort the critical lines and caustics of the lens (see Figures 6 and 7). They do not, however, solve the problem that the model for the radio ring is slightly rounder than observed. Presumably, the solution lies in using models with both the external galaxies and an ellipsoidal model of the lens galaxy, since Keeton et al. (1997) found that such models generically produced good fits to the four-image lens systems. Such lens models for extended sources are computationally expensive and are beyond the scope of this paper. However, we deem our models adequate for the current purpose of understanding the basic structure of the MG 1131+0456 lens system.

3.2. Reconstructing the Extended Source Components

We now fit the H, I, and R images using a de Vaucouleurs model of fixed structure for the *light* from the lens galaxy and the lensing mass distribution from §3.1 to produce lensed images of the models for the extended emission of the host galaxy. The H band ring is well modeled as the image of an exponential disk offset from the radio core. The intrinsic magnitude of the exponential disk is $H = 19.6$ mag with a scale length of $R_d = 0''.29$, axis ratio 0.69 and major axis PA of 70° . The axis ratio corresponds to an inclination angle of 44° (where 90° is face-on). For comparison, the intrinsic magnitude of the source corresponding to the radio core is $H = 22.8$ mag. The core component is offset by $0''.2$ to the Northwest of the center of the exponential disk. The residuals from this model consisted of excess emission on the Northeast side of the ring, which we could model and subtract by the addition of several extended Gaussian components to the source model with a total magnitude of $H = 21.9$ mag. The total magnitude of all the source components was $H = 19.3$ mag, which we see as a ring with a total magnitude of $H = 17.4$ mag. Figure 6 shows the ring structures after subtracting the best fitting model of the lens galaxy, and Figure 7 shows the reconstruction of the unlensed source. We clearly see the offset between the

peak of the extended stellar emission and the AGN core. The major axis of the radio jet is roughly perpendicular to the offset vector.

The I and R rings are both more complicated in structure and significantly noisier, so it is difficult to evaluate which small scale substructures of the optical ring are real. We decided to use a smoothed version of the image (as shown in Figures 5 and 6) to enhance the low surface brightness images of the host galaxy. The key geometric fact is that the extended arc seen in the I image (Figure 6) running from South of the lens to the Northeast predicts the compact piece of the ring seen to the West of the lens. Similarly, the gaps in the ring near the locations of both radio cores correspond to lensed images of the same source regions. No counterparts of the radio cores are visible in the optical images. *The structural features of the optical ring are features intrinsic to the host galaxy rather than features produced by absorption in the lens galaxy.*

Since the optical ring corresponds to only portions of the infrared ring, we modeled the source by a grid of ~ 300 extended Gaussians whose parameters were optimized to match the observations. The model correctly reproduces the ring structure but is limited by the poor signal-to-noise ratio between the ring and the background. Figure 7 shows the reconstructions of the source morphology in I and R. The intrinsic magnitudes of the host are $I=23.2$ mag and $R=23.8$ mag. The R and I-band flux comes mostly from the SE half of the host galaxy, with a sharp drop in the emission starting near the peak of the extended IR emission and extending over the location of the AGN core. The changing morphology of the lens between the optical and the infrared appears to be entirely created by changes in the morphology of the source. Much of the optical emission lies along the radio jet axis, which is suggestive of the alignment effect (McCarthy et al. 1987). Assuming $z_s > 2$, the aligned emission represents UV rest-frame light. If MG 1131+0456 is typical of other high redshift, high luminosity radio sources, the alignment is caused by a combination of off-axis scattering of the core light and jet-induced shocks in the ISM of the host galaxy (Tadhunter et al. 1992, van Breughel et al. 1985).

Alternatively, the geometry is suggestive of an AGN embedded in a larger, dusty stellar disk (e.g. Centaurus A). The infrared source is relatively well modeled as an exponential disk at an inclination near 45° with the far side of the disk in the Southeast quadrant. Qualitatively, at least, such a geometry could both hide half the galaxy at the shorter optical wavelengths and produce an offset between the radio core and the apparent center of the host galaxy. The peak of the extended emission does appear to steadily shift to the Southeast for the bluer wavelengths. The reconstructed morphology of the optical source does not perfectly correspond to such a model, but the data used for the reconstructions are also poor. The complicated morphology, the quality of the optical data, and the lack of a source redshift make it impossible to interpret the colors of the source in detail. The average color is “bluish” in the optical, with $R-I \simeq 0.6 \pm 0.3$ mag, and red from the optical to the infrared, with $R-H \simeq 3.9 \pm 0.3$. Larkin et al. (1994) found that the brightness of the source increased dramatically between J and H, but modestly between H and K which

suggests that the source redshift is above 1.8 and below 3.0 if we assume that the spectrum has a break near 4000 Å. The mean colors of the source are roughly consistent with a stellar population at $z_s > 2$ (see Figure 4), but they impossible to interpret in detail without a good model for the effects of the dust in the source on the fluxes. We obtain a similar estimate of $z_s \gtrsim 2$ if we require the lens galaxy to lie on the fundamental plane (either fixing the lens redshift to the Hammer et al. (1985) value or performing a simultaneous estimate).

4. Consequences of the Limits on the Dust Content of the Lens

The residuals in modeling the H-band ring provide the best means of limiting the amount of differential extinction produced by the lens galaxy. The surface brightness of the source is unaffected by lensing, so any residuals in the H image are a combination of noise, shortcomings in either the photometric or lens model, and differential extinction. The fractional residuals f in the H image are related to the differential extinction by $\Delta E(B - V) = (5f/R_{F160W} \ln 10)(1 + f^3/3 + \dots) \simeq 1.2f$ over the multiply-imaged region. Figure 8 shows the fractional residuals (modestly smoothed) for the regions exceeding 10% of the peak flux in the ring. Our model makes the smallest errors in the bright parts of the ring, where $|f| \lesssim 5\%$, and then rises near the edges where we reach the limits of our parameterization of the surface brightness distribution. Thus over the region from $0''.5 \lesssim R \lesssim 1''.5$ from the lens center ($R_e \lesssim R \lesssim 3R_e$ or $3h_{65}^{-1}\text{kpc} \lesssim R \lesssim 10h_{65}^{-1}\text{kpc}$) the extinction varies by less than $\Delta E(B - V) \lesssim 0.06$. For the patchy extinction seen in most galaxies, such a limit on the differential extinction essentially corresponds to a comparable limit on the mean extinction. Note that this test is also sensitive to patchy, but grey extinction. A smoothly distributed dust component with a significant optical depth, such as $E(B - V) = E_0 e^{-R/R_0}$, must have an enormous scale length to keep the ring colors as uniform as observed. The limit roughly corresponds to $R_0 > 100E_0 h_{65}^{-1} \text{ kpc}$, which is implausible for high optical depths given a stellar scale length of only $6h_{65}^{-1} \text{ kpc}$. Figures 3 and 4 also show the source reddening vector given up to $E(B - V) = 1$ mag of extinction in the lens galaxy. Given the observed source flux, the implied intrinsic source luminosity becomes implausibly large if the lens contains any significant amount of extinction.

The existence of the infrared rings in both MG 1131+0456 and B 1938+666 (King et al. 1998) means that the Malhotra et al. (1997) and Larkin et al. (1994) hypothesis that the red color of the lenses is created by dust in the lens galaxy is ruled out. In fact, the Annis & Luppino (1993) hypothesis that the red color is created by dust in the source galaxy obscuring the AGN combined with emission by the stars in the host galaxy is correct for both systems. Only MG 0414+0534 is left as a candidate for a very dusty, early-type lens. While the quasar spectra in MG 0414+0534 are very reddened (Lawrence et al. 1995), the differential extinction between the four lines of sight is less than 10% of the total (McLeod et al. 1998a) even though the paths are separated by $\sim 5 \text{ kpc}$. Such uniformity in the interstellar medium of the lens galaxy seems implausible given the observed properties of

nearby galaxies. In fact, the discovery of the extended blue arc connecting the brighter three quasar images in MG 0414+0534 (Falco et al. 1997) also rules out the dusty lens hypothesis in this system. The arc is already bluer than the lens galaxy and has an estimated intrinsic luminosity of $\sim 0.5L_*$ before any correction for dust in the lens galaxy. If the extinction in the lens was genuinely $A_V \sim 7$ mag, then the arc color would be remarkably blue and the total arc luminosity phenomenal. It is important to include the large Galactic extinction of $E(B - V) = 0.30$ mag (Schlegel, Finkbeiner & Davis 1998) towards MG 0414+0534, because it is largely responsible for the anomalously red color of the lens galaxy.

These results do not imply, however, that complete absence of dust in lens galaxies. Falco et al. (1997) demonstrated that reconciling the statistics of optical and radio lens samples required dust in even the early-type galaxies. They estimated a mean extinction for the early-type lens galaxies of $A_B = 0.5 \pm 0.4$ mag in the observers frame, and that spiral galaxy lenses may be completely eliminated from the quasar sample. The cosmological limits purely from the radio-selected sample were $\lambda_0 < 0.65$ at $2\text{-}\sigma$ in flat cosmological models, so the effects of extinction provided no escape from the lensing constraints on the cosmological constant. Falco et al. (1997) also noted that the composition of the typical optical counterparts of flat-spectrum radio sources changed rapidly below 250 mJy (at 8 GHz), from over 90% quasars at brighter fluxes to approximately 50% at 50 mJy. Hence the source population from which the radio lenses are drawn is qualitatively different from that of bright radio sources. Although MG 1131+0456 appears to be nearly transparent, several other systems are known to contain significant quantities of molecular gas and produce large differential extinctions of the lensed images. The two lenses with the largest differential extinctions, PKS 1830–211 with $\Delta E(B - V) \simeq 2.9$ mag and B 0218+357 with $\Delta E(B - V) \simeq 0.8$, are also the two lenses in which significant column densities of molecular gas are detected in absorption (see Gerin et al. 1997 and references therein). The remaining lenses appear to have far more modest differential extinctions (see Lehár et al. 1998).

5. SUMMARY

By combining NICMOS and WFPC2 HST images in R, I, and H of MG 1131+0456 with the existing 8 GHz radio maps, we have been able to construct a comprehensive picture of both the source and the lensing structures in the system. Our new data show that a correct interpretation of the system has not been possible on the basis of lower resolution data. In particular, we find that the host galaxy of the source AGN is the dominant component of the H-band flux. On the basis of these new data and of extensive modeling we have been able to establish the following results:

- (1) The very red optical – IR colors of the lensed source are due to the extended flux from the source host galaxy at $z_{source} > 2$. They are *not* due to dust reddening of the AGN at either the source or the lens redshift. In addition, there is direct evidence from our data

that the MG 1131+0456 lens galaxy is indeed nearly transparent, in contrast to earlier inferences by Larkin et al. (1994) and Malhotra et al. (1997). The second reddest lens, B 1938+666, shows very similar properties (King et al. 1998), although the smaller angular size and more comparable luminosities of the lens galaxy and the ring make it more difficult to model the system in detail. Thus we conclude that the dusty lens hypothesis of Larkin et al. (1994) and Malhotra et al. (1997) is invalid.

(2) The new images have allowed us to establish the correct R, I and H magnitudes for the lens galaxy and its two close neighbors. These data corroborate that the lens is a member of a galaxy group, or poor cluster, at $z_l \simeq 0.85$. The measured effective radius, luminosity and mass of the main lens galaxy make it one of the highest redshift galaxies that can be put on the Fundamental Plane. The two neighboring galaxies (C and D) now have just the right luminosities and positions to induce the required lensing shear, both in direction and in amplitude. This intermediate density lens environment is similar to that of many other lenses (e.g. MG 0751+2716 (Lehár et al. 1997), Q 0957+561 (Young et al. 1981), PG 1115+080 (Impey et al. 1998), and B 1422+231 (Yee and Ellingson, 1994)).

(3) Using the lens model derived from the radio data, we reconstruct the source structure at R, I, and H. The bright H band ring ($m_H \simeq 17.4$ mag!) is almost completely modeled as the image of an inclined (45°) exponential disk with a point source at the location of the radio core. The radio core is offset by $0''.2$ NW of the center of the extended emission. The reconstructed source images in R and I however, show a severe flux deficit on the NW side of the center, which appear in the observations as gaps in the optical rings. We argue that this morphology could arise from embedding the source in a larger, thin dusty disk (e.g. Centaurus A).

Few high redshift, red galaxies have been studied in detail because of the difficulties in studying them spectroscopically. The complicated source morphology of MG 1131+0456 is not consistent with the simple model of an old stellar population at intermediate redshift that seems to explain LBDS 53W091. It could be consistent with the dust obscured star formation model that explains HR 10. A good infrared spectrum of the source or high resolution images of the source at J and K to complement our H band images will be required to understand the source in greater detail. Although NICMOS imaging is preferred, new, high resolution ground-based images may suffice because the H band morphology can be used as a template for understanding any new data.

Support for the CASTLES project was provided by NASA through grant numbers GO-7495 and GO-7887 from the Space Telescope Science Institute, which is operated by the Association of Universities for Research in Astronomy, Inc. CSK and CRK were also supported by the NASA Astrophysics Theory Program grant NAG5-4062. HWR is also supported by a Fellowship from the Alfred P. Sloan Foundation.

REFERENCES

- Annis, J., 1992, *ApJL*, 391, L17
- Annis, J. & Luppino, G.A., 1993, *ApJL*, 407, L69
- Bertin, E. & Arnouts, S., 1997, *A&AS*, 117, 393
- Bruzual, G., & Charlot, S., 1993, *ApJ*, 405, 538
- Cardelli, J.A., Clayton, G.C., & Mathis, J.S., 1989, *ApJ*, 345, 245
- Chen, G. & Hewitt, J.N., 1993, *AJ*, 106, 1719
- Chen, G., Kochanek, C.S. & Hewitt, J.N., 1995, *ApJ*, 447, 62
- Dey, A., Spinrad, H. & Dickenson, M., 1995, *ApJ*, 440, 515
- Dunlop, J. S., Peacock, J., A., Spinrad, H., Dey, A., Jimenez, R., Stern, D., & Windhorst, R. A. 1996, *Nature*, 381, 581
- Eisenhardt, P.R., Armus, L., Hogg, D.W., Soifer, B.T., Neugebauer, G. & Werner, M.W., 1996, *ApJ*, 461, 72
- Ellis, R.S., Smail, I., Dressler, A., Couch, W.J., Oemler, A., Butcher, H. & Sharples, R.M., 1997, *ApJ*, 483, 582
- Faber, S.M., & Jackson, R.E., 1976, *ApJ*, 204, 668
- Falco, E.E., Kochanek, C.S. & Muñoz, J.A., 1998, *ApJ*, 494, 47
- Falco, E.E., Lehár, J. & Shapiro, I.I., 1997, *AJ*, 113, 540
- Fall, S.M. & Pei, Y.C., 1993, *ApJ*, 402, 479
- Fassnacht, C.D., Womble, D.S., Neugebauer, G., Browne, I.W.A., Readhead, A.C.S., Matthews, K. & Pearson, T.J., 1996, *ApJL*, 460, L103
- Gerin, M., Phillips, T.G., Benford, D.J., Young, Y.H., Menten, K.M., & Frye, B., 1997, *ApJL*, 488, 31
- Graham, J.R., & Dey, A., 1996, *ApJ*, 471, 720
- Guiderdoni, B., & Rocca-Volmerange, B., 1988, *A&AS*, 74, 185
- Hammer, F., Angonin, M.C., Le Fevre, O., Meylan, G., Smette, A. & Surdej, J., 1991, *A&A*, 250, L5
- Heisler, J., & Ostriker, J.P., 1988, *ApJ*, 332, 543

- Hewitt, J.N., Turner, E.L., Schneider, D.P., Burke, B.F. & Langston, G.I., 1988, *Nature*, 333, 537
- Hewitt, J.N., Turner, E.L., Lawrence, C.R., Schneider, D.P. & Brody, J.P., 1992, *AJ*, 104, 968
- Hewitt, J.N., Chen, G.H., & Messier, M.D., 1995, *AJ*, 109, 1956
- Holtzman, J.A., Burrows, C.J., Casertano, S., Hester, J.J., Trauger, J.T., Watson, A.M., & Worthey, G., 1995, *PASP*, 107, 1065
- Impey, C.D., & Neugebauer, G. 1988, *AJ*, 95, 307
- Impey, C.D., Falco, E.E., Kochanek, C.S., Lehár, J., McLeod, B.A, Rix, H.-W., Peng, C.Y. & Keeton, C.R., 1998, *ApJ*, December 20
- Jackson, N., de Bruyn, A.G., Myers, S., Bremer, M.N., Miley, G.K., Schilizzi, R.T., Browne, I.W.A., Nair, S., Wilkinson, P.N., Blandford, R.D., Pearson, T.J. & Readhead, A.C.S., 1995, *MNRAS*, 274, L25
- Jorgensen, I., Franx, M. and Kjaergard, P., 1992, *A&AS*, 95, 489
- Keeton, C. R, Kochanek, C. S., & Falco, E. E., 1988, *astro-ph/9708161*
- Keeton, Kochanek & Seljak 1997] Keeton, C.R., Kochanek, C.S., & Seljak, U. 1997, *ApJ*, 482, 604
- Kelson, D., van Dokkum, P, Franx, M., Illingworth, G. & Fabricant, D., 1997, *ApJ*, 478, L13.
- King, L.J., Jackson, N.J., Blandford, R.D., Bremer, M.N., Browne, I.W.A., de Bruyn, A.G., Fassnacht, C., Koopmans, L., Marlow, D., Nair, S. & Wilkinson, P.N., 1997, *astro-ph/9710171*
- King, L.J., Browne, I.W.A., Muxlow, T.W.B., Narasimha, D., Patnaik, A.R., Porcas, R.W., & Wilkinson, P.N., 1997, *MNRAS*, 298, 450
- Kochanek, C.S., Blandford, R.D., Lawrence, C.R. & Narayan, R., 1989, *MNRAS*, 238, 43
- Larkin, J.E., Matthews, K., Lawrence, C.R., Graham, J.R, Harrison, W., Jernigan, G., Lin, S., Nelson, J., Neugebauer, G., Smith, G., Soifer, B.T. & Ziomkowski, C., 1994, *ApJL*, 420, L9
- Lawrence, C.R., Elston, E., Januzzi, B.T. & Turner, E.L., 1995, *AJ*, 100, 2570
- Lehár, J., Falco, E.E., Impey, C.D., Kochanek, C.S., McLeod, B.A., Rix, H.-W., C.R., Keeton, & Muñoz, J.A., 1998, in preparation

- Malhotra, S., Rhoads, J.E. & Turner, E.L., 1997, MNRAS, 288, 138
- McCarthy, P.J., van Breughel, W., Spinrad, H., & Djorgovski, S. 1987, ApJ, 321, L29
- McLeod, B. A., 1997, in 1997 HST Calibration Workshop, ed S. Casertano et al.
- McLeod, B.A., Bernstein, G.M., Rieke, M.J., & Weedman, D.W., 1998a, AJ, 115, 1377
- McLeod, B.A., Falco, E.E., Impey, C.D., Kochanek, C.S., Lehár, J., Rix, H.-W., C.R., Keeton, & Muñoz, J.A., 1998b, in preparation
- Moustakas, L.A., Davis, M., Graham, J.R., Silk, J., Peterson, B.A., & Yoshii, Y., 1997, ApJ, 475, 445
- Nadeau, D., Yee, H.K.C., Forrest, W.J., Garnett, J.D., Ninkov, Z. & Pipher, J.L., 1991, ApJ, 376, 430
- Rhoads, J.E., Malhotra, S., & Kundic, T., 1996, AJ, 111, 642
- Schlegel, D.J., Finkbeiner, D.P., & Davis, M., 1998, ApJ, 500, 525
- Spinrad, H., Dey, A., Stern, D., Dunlop, J., Peacock, J., Jimenez, R. & Windhorst, R., 1997, ApJ, 484, 581
- Stanford, S.A., Eisenhardt, P.R. & Dickinson, M., 1995, ApJ, 440, 515
- Stanford, S.A., Eisenhardt, P.R. & Dickinson, M., 1998, ApJ, 492, 461
- Tadhunter, C. Scarrott, S., Draper, P., & Rolph, C. 1992, MNRAS, 256, 53
- van Breughel, W., et al. 1985, ApJ, 290, 496
- van Dokkum, P.G., Franx, M., Kelson, D.D., & Illingworth, G.D., 1998, ApJL, 504, 17
- Webster, R.L., Francis, P.J., Peterson, B.A., Drinkwater, M.J. & Masci, F.J., 1995, Nature, 375, 469
- Wills, B.J., Wills, D., Evans, N.J., Natta, A., Thompson, K.L., Breger, M. & Sitko, M.L., 1992, ApJ, 400, 96
- Witt, A., Thronson, H., and Capuano, J., 1992, ApJ, 393, 611.
- Yee, H. and Ellingson, E., 1994, AJ, 107, 28.
- Young, P., Gunn, J., Oke, J., Westphal, J., Kristian, J., 1981, ApJL, 244, 736.

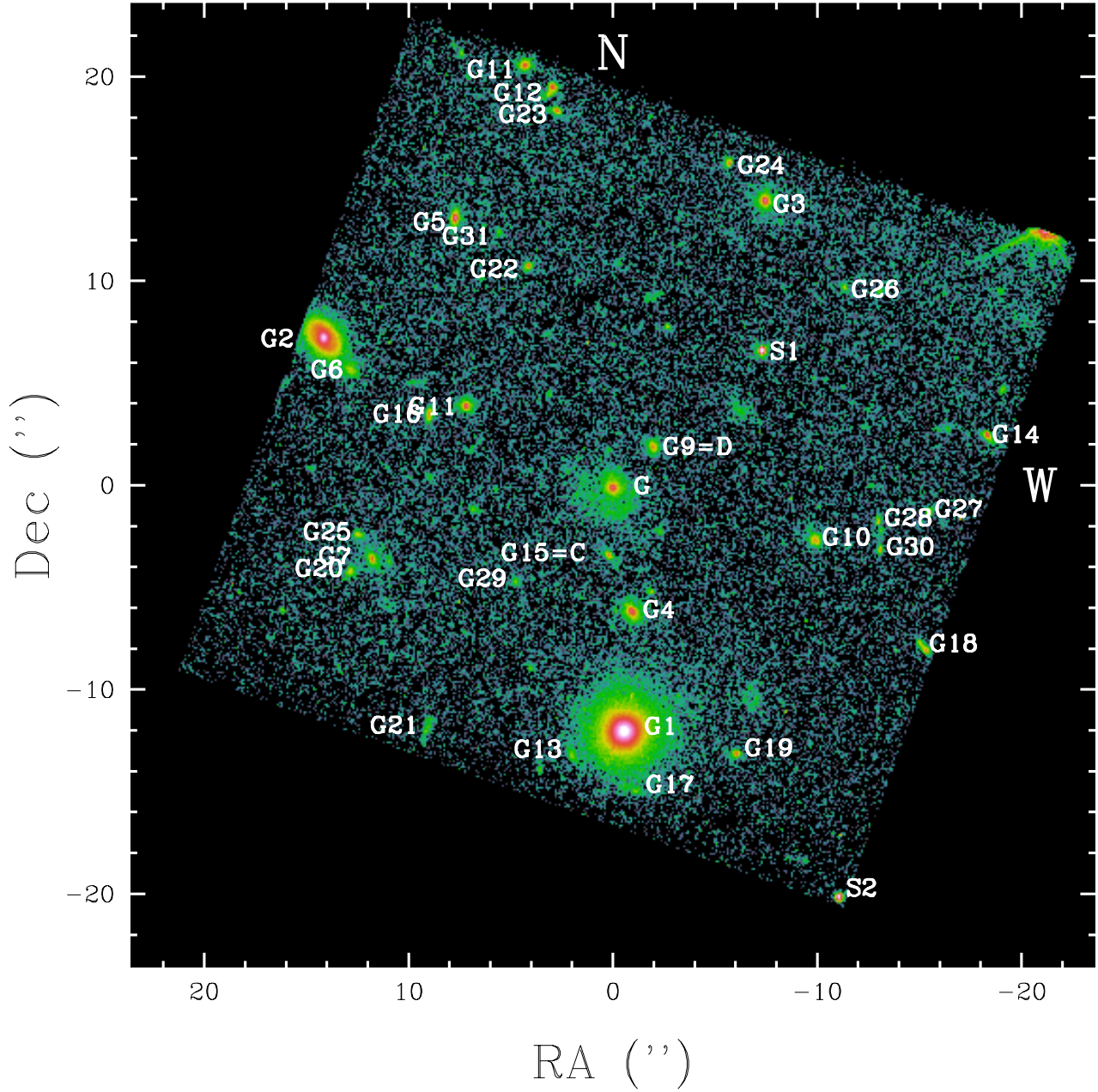


Fig. 1.— Coadded I and R PC images of MG 1131+0456 . Objects brighter than $I < 25$ mag are labeled as they appear in Table 1.

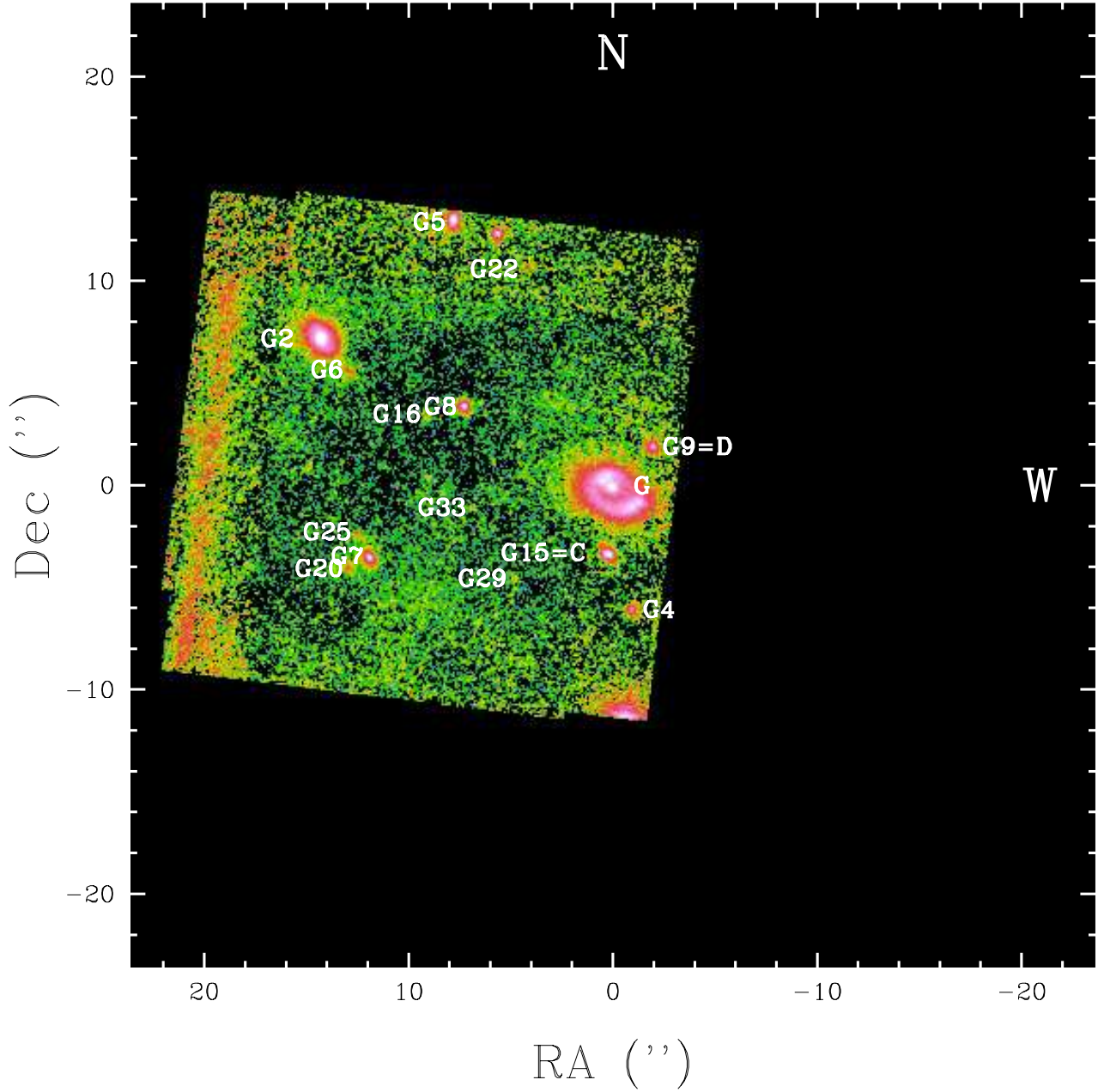


Fig. 2.— NICMOS H image of MG 1131+0456 . Objects brighter than $I < 25$ mag are labeled as they appear in Table 1. The noise increases greatly at the edges where the image is the sum of fewer dithered sub-images.

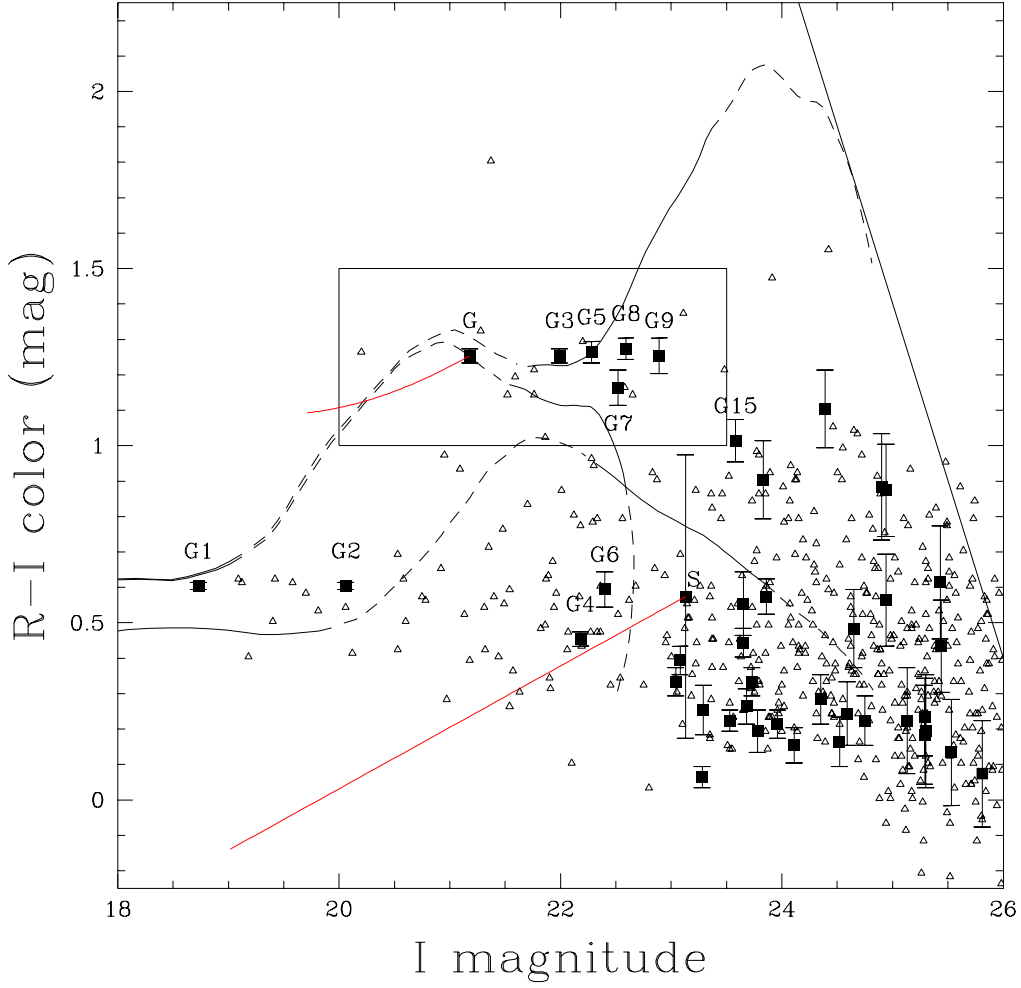


Fig. 3.— R–I versus I color magnitude diagram. The filled squares mark the galaxies found in the PC image, and the smaller triangles mark the galaxies found in the surrounding WF images. The diagonal line on the right edge of the distribution shows the detection threshold created by the R flux limit. The three curves show the magnitude and color of an L_* galaxy in the burst (top), E/S0 (middle), and Sc (bottom) spectrophotometric models. The line style shifts from solid to dashed every $\Delta z = 0.5$ ($z < 0.5$ solid, $0.5 < z < 1$ dashed \dots). A brighter (fainter) galaxy would lie to the left (right) of the curve at a fixed color. The box shows the region used to quantify the presence of the lensing group in §2.5. The effects of dereddening uniformly mixed dust within the lens (up to $E(B - V) = 1$ mag) is shown by the line extending from the primary lens G, and the effects of the same dust on the source by an analogous line starting at S. All magnitudes are corrected for the estimated foreground Galactic extinction.

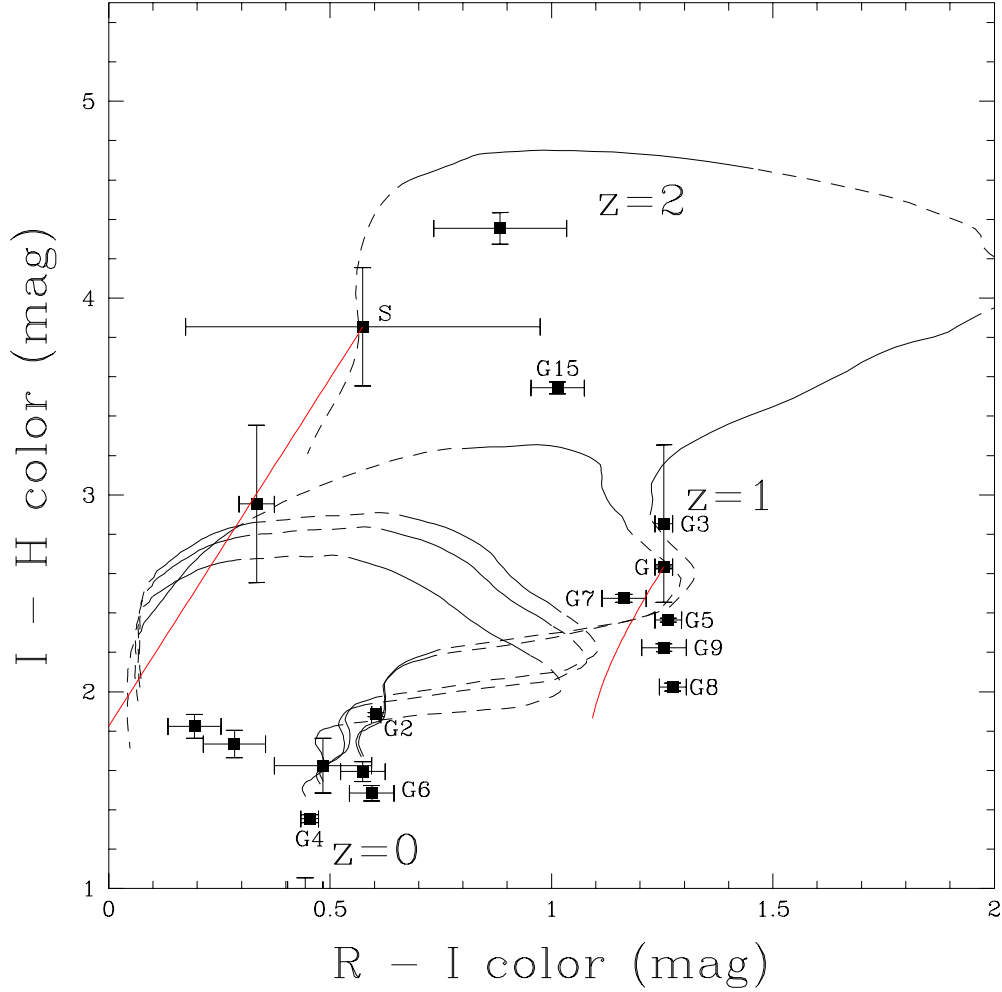


Fig. 4.— I-H versus R-I color-color diagram for the galaxies found in the NIC2 image with $I < 25$ mag. The five curves are the colors of the initial burst, E/S0, Sa, Sb, and Sc galaxy models. The line pattern shifts from solid to dashed every $\Delta z = 0.5$. The curve extending from the point for the primary lens G shows the effects of dereddening the lens galaxy by up to $E(B - V) = 1$ magnitudes of uniformly mixed dust, and the curve extending from source (labeled S) shows the effect of the same dust on the source. All magnitudes are corrected for the estimated foreground Galactic extinction.

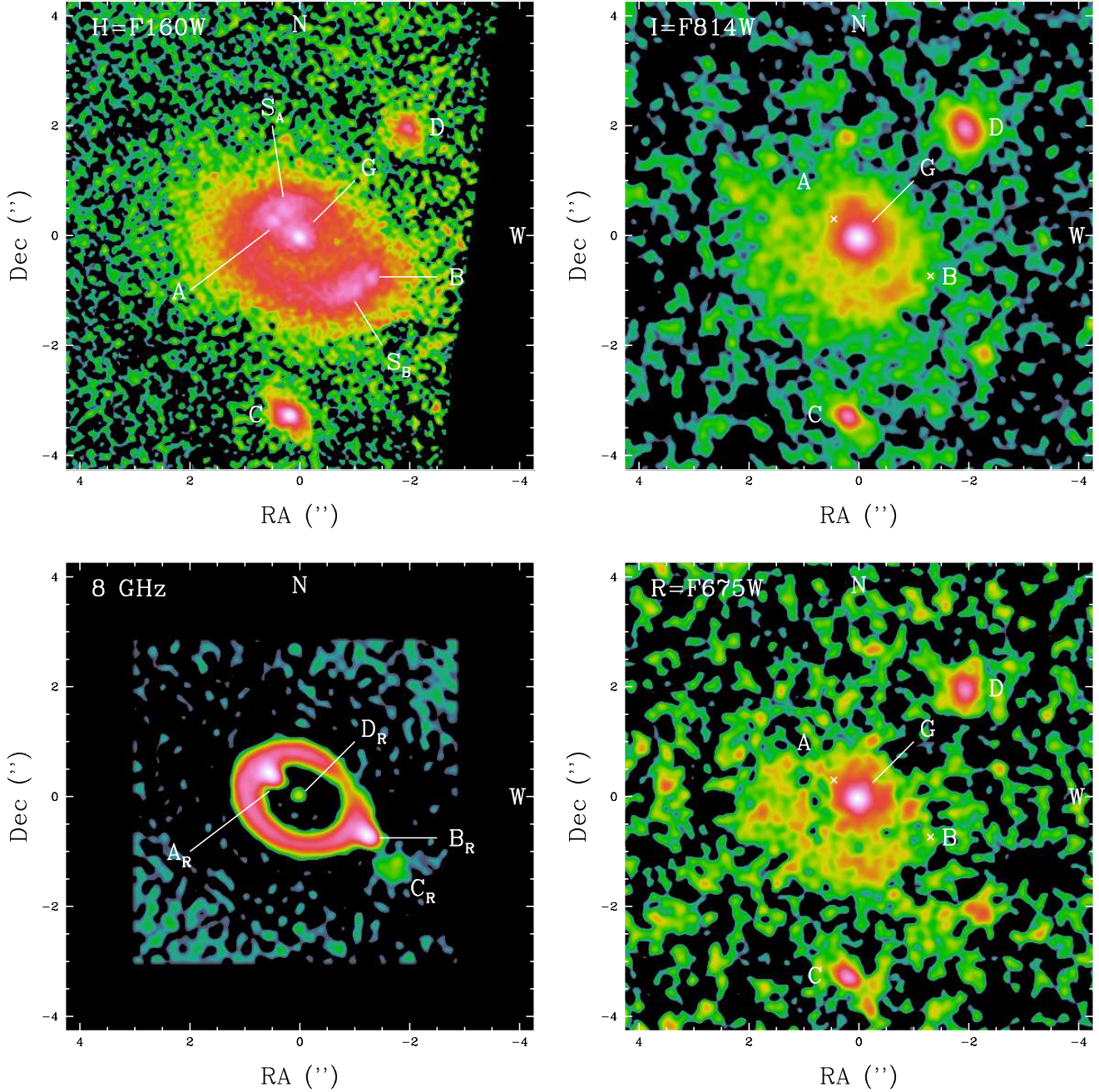


Fig. 5.— Close-ups of the H (top-left), I (top-right), R (bottom-right) and 8 GHz radio map (bottom-left, from Chen & Hewitt 1993) images. The I and R images have been smoothed to make the ring clearly visible. The AGN cores are located at A and B (A_R and B_R in the radio image) and they are marked by the crosses in the I and R images where no core component is directly visible. The radio image was registered with the optical by centering ring component D_R on the lens galaxy G.

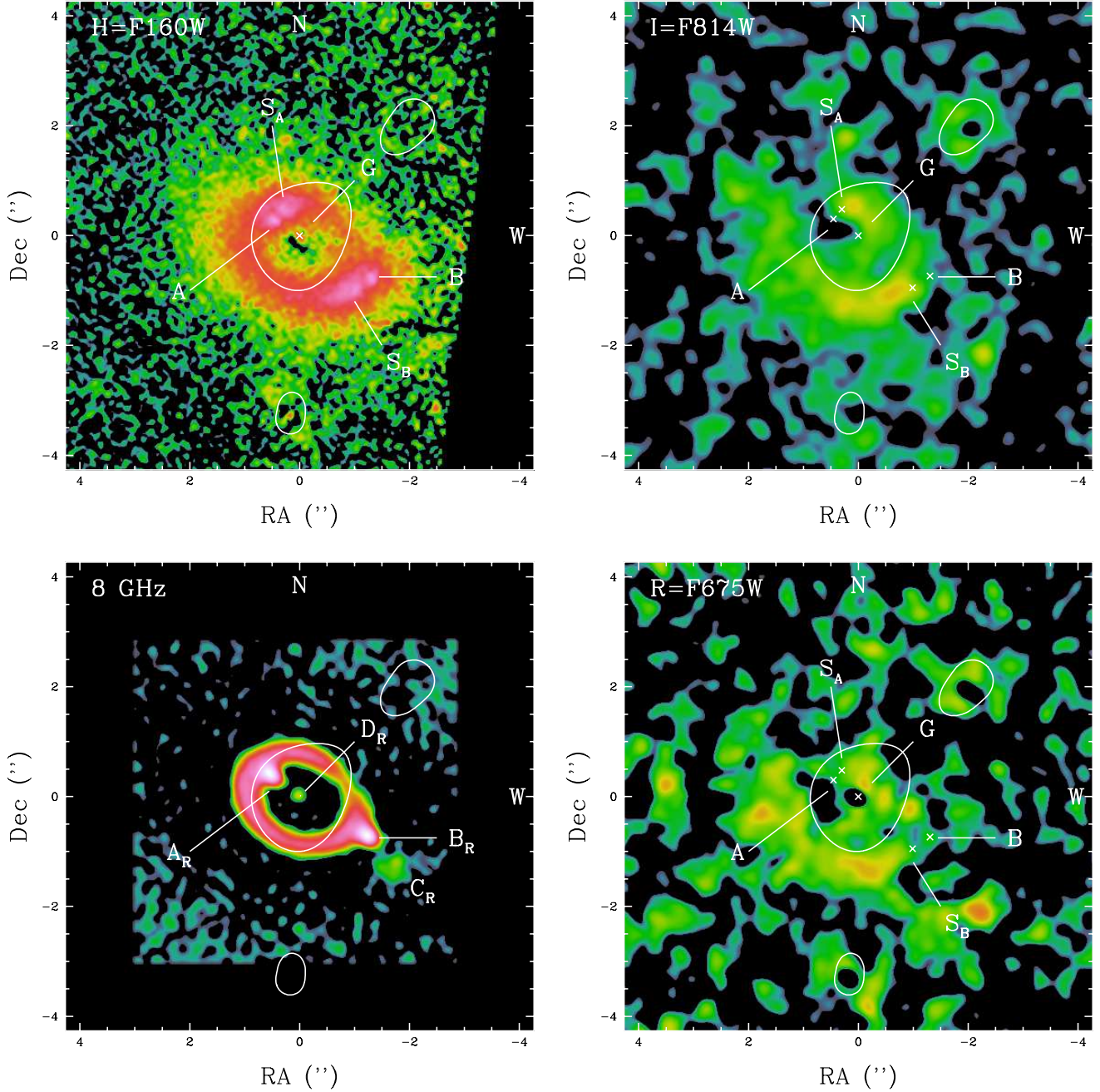


Fig. 6.— Close-ups of the ring at H (top-left), I (top-right), R (bottom-right) and 8 GHz radio map (bottom-left, from Chen & Hewitt 1993) after subtracting the best fit galaxy model. The I and R images have been smoothed to make the ring clearly visible. The contours show the critical lines of the lens model.

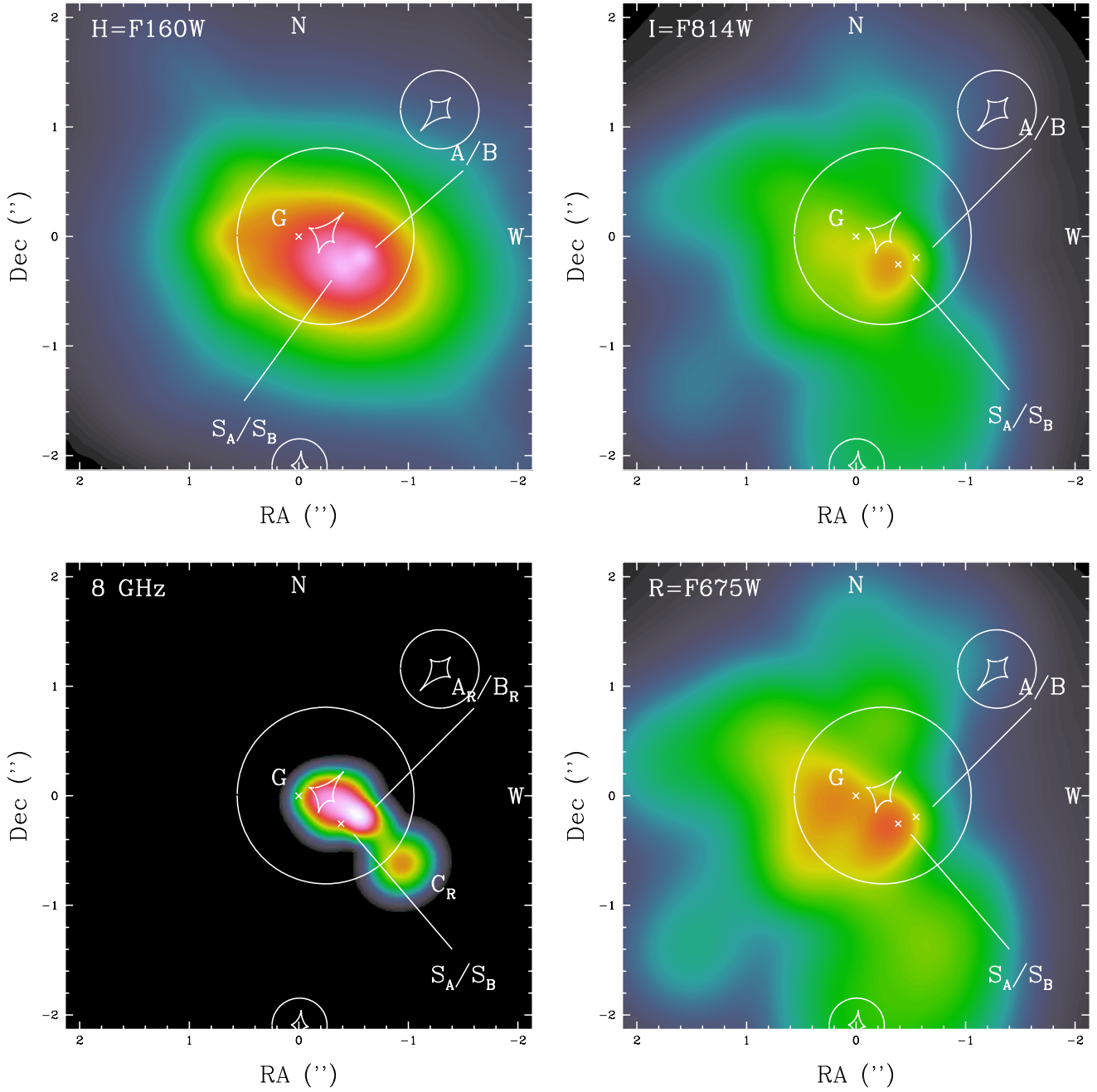


Fig. 7.— Source reconstructions at H (top-left), I (top-right), R (bottom-right) and 8 GHz. The I and R reconstructions used the smoothed images. The contours show the caustics of the lens model.

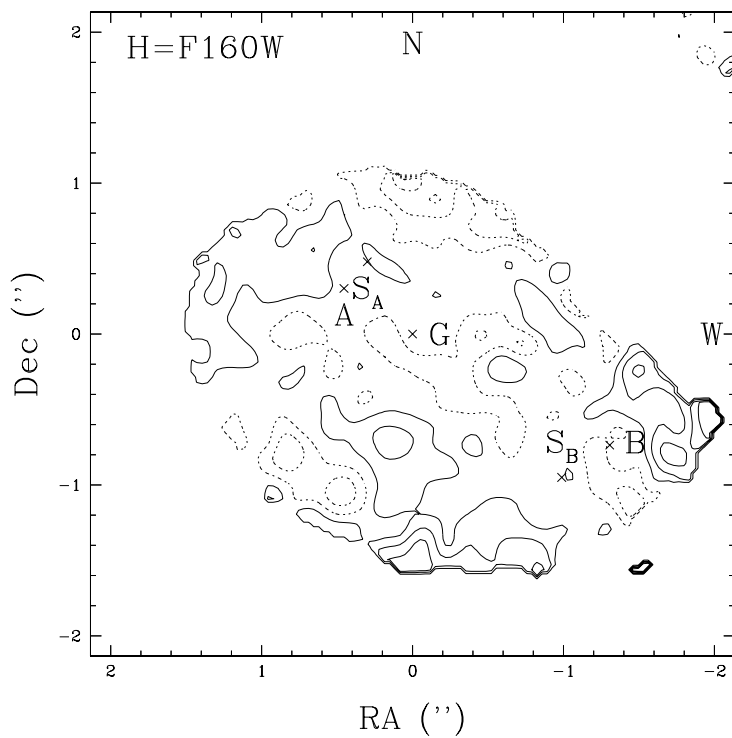


Fig. 8.— Fractional ring residuals over the region with surface brightness exceeding 10% of the peak surface brightness. The differential extinction in the lens galaxy must satisfy $\Delta E(B - V) \leq 1.2f$. The solid contours are drawn at $f = 5\%$, 15%, 25%, and 35%, and the dashed contours are drawn at $f = -5\%$, -15%, -25%, and -35%. Most of the infrared ring, including the regions corresponding to the gaps in the optical ring lie in the $|f| < 5\%$ region.

Table 1. Objects Near MG 1131+0456

ID	RA(")	Dec (")	I (mag)	R-I (mag)	I-H (mag)	γ_T	Comments
G1	-0.5	-11.7	18.80 ± 0.01	0.63 ± 0.01		0.113	
G2	13.9	7.2	20.13 ± 0.01	0.63 ± 0.01	1.93 ± 0.01	0.046	
G	0	0	21.04 ± 0.01	1.26 ± 0.02	2.81 ± 0.01		Lens Galaxy
S1	-7.2	6.6	21.87 ± 0.01	1.15 ± 0.01	(1.5 ± 0.4)		Star, A-6
G3	-7.3	13.8	22.06 ± 0.01	1.28 ± 0.02	(2.9 ± 0.4)	0.019	Lens Group, A-5
G4	-0.9	-6.0	22.25 ± 0.02	0.48 ± 0.02	1.40 ± 0.02	0.045	A-8
G5	7.6	13.0	22.35 ± 0.01	1.29 ± 0.03	2.41 ± 0.01	0.017	Lens Group, A-3
S2	-10.9	-19.7	22.45 ± 0.01	1.36 ± 0.02			Star
G6	12.7	5.7	22.47 ± 0.03	0.62 ± 0.05	1.53 ± 0.04	0.018	
G7	11.6	-3.4	22.59 ± 0.03	1.19 ± 0.05	2.52 ± 0.02	0.019	Lens Group, A-1
G8	7.1	4.0	22.66 ± 0.02	1.30 ± 0.03	2.07 ± 0.02	0.028	Lens Group, A-9
G9	-1.9	2.0	22.96 ± 0.03	1.28 ± 0.05	2.27 ± 0.02	0.071	Lens Group, A-D
G10	-9.7	-2.5	23.11 ± 0.04	0.36 ± 0.04	(3.0 ± 0.4)	0.018	A-7
G11	4.2	20.4	23.15 ± 0.03	0.42 ± 0.04		0.009	
G12	3.0	19.2	23.35 ± 0.03	0.09 ± 0.03		0.008	
G13	2.0	-12.8	23.36 ± 0.05	0.28 ± 0.07		0.013	
G14	-18.0	2.5	23.60 ± 0.03	0.25 ± 0.03		0.008	
G15	0.2	-3.3	23.65 ± 0.04	1.04 ± 0.06	3.59 ± 0.03	0.043	Lens Group, A-C
G16	8.9	3.5	23.72 ± 0.04	0.47 ± 0.04	1.04 ± 0.06	0.014	
G17	-1.1	-14.6	23.72 ± 0.05	0.58 ± 0.09		0.009	
G18	-15.0	-7.7	23.75 ± 0.04	0.29 ± 0.05		0.008	
G19	-5.9	-12.8	23.80 ± 0.04	0.36 ± 0.04		0.009	
G20	12.7	-4.0	23.85 ± 0.06	0.22 ± 0.06	1.87 ± 0.06	0.010	
G21	9.0	-11.6	23.90 ± 0.06	0.93 ± 0.11		0.009	
G22	4.1	10.7	23.93 ± 0.04	0.60 ± 0.05	1.64 ± 0.05	0.011	
G23	2.7	18.2	24.03 ± 0.05	0.24 ± 0.04		0.006	
G24	-5.6	15.7	24.18 ± 0.05	0.18 ± 0.05		0.007	
G25	12.3	-2.2	24.42 ± 0.06	0.31 ± 0.07	1.78 ± 0.07	0.008	
G26	-11.2	9.6	24.46 ± 0.07	1.13 ± 0.11		0.007	
G27	-15.2	-1.2	24.59 ± 0.07	0.19 ± 0.07		0.006	
G28	-12.8	-1.6	24.66 ± 0.08	0.27 ± 0.09		0.007	
G29	4.7	-4.5	24.72 ± 0.09	0.51 ± 0.11	1.67 ± 0.14	0.013	
G30	-12.9	-3.0	24.82 ± 0.07	0.25 ± 0.07		0.006	
G31	5.5	12.3	24.97 ± 0.09	0.91 ± 0.15	4.40 ± 0.08	0.006	A-4
G32	7.3	21.0	25.01 ± 0.10	0.90 ± 0.13		0.003	
G33	6.7	-1.0	25.01 ± 0.09	0.59 ± 0.13	1.49 ± 0.14	0.011	
G34	10.8	-3.5	25.20 ± 0.13	0.25 ± 0.15	< 1.77	0.006	

Table 1—Continued

ID	RA (")	Dec (")	I (mag)	R-I (mag)	I-H (mag)	γ_T	Comments
G35	-2.3	-2.1	25.36 ± 0.12	0.21 ± 0.14	2.43 ± 0.12	0.021	
G36	-18.8	4.7	25.36 ± 0.12	0.26 ± 0.11		0.003	
G37	-18.6	9.5	25.37 ± 0.12	0.22 ± 0.16		0.003	
G38	4.0	-8.7	25.50 ± 0.13	0.64 ± 0.16	< 1.65	0.006	
G39	-12.9	9.5	25.51 ± 0.12	0.46 ± 0.13		0.004	
G40	-1.8	-5.0	25.58 ± 0.10	-0.07 ± 0.17	-0.09 ± 0.81	0.011	
G41	3.5	-13.6	25.60 ± 0.14	0.16 ± 0.15		0.004	
S3	-2.6	7.8	25.60 ± 0.11	0.18 ± 0.09	2.21 ± 0.10		Star
G42	15.9	-5.9	25.88 ± 0.12	0.10 ± 0.15	< 1.83	0.003	

Note. — SExtractor (Bertin & Arnouts 1997) magnitudes and colors numbered in order of decreasing I magnitude. The primary lens galaxy is labeled G, the other galaxies and the stars in the PC field are labeled G1, G2 ... and S1, S2 ... respectively in order of decreasing I magnitude. The lens galaxy, probable lens group members and stars are marked. The labels A-? give the label of the object from Annis (1992). Where we lack an H magnitude and Annis (1992) measured a K' magnitude, we include an estimated I-H magnitude in parentheses using the mean H-K' magnitude for the objects we have in common. The parameters for the primary lens G are the estimates from SExtractor, which may be biased by the ring. For comparison the fitted values from §2.4 are I=21.25 mag, R-I=1.28, and I-H=2.68 mag respectively. The γ_T column is the estimated external shear the galaxy would add to the lens model assuming the galaxies are singular isothermal spheres at the same redshift obeying the Faber-Jackson (1976) relation (see §2.5).